

Generative models for two-ground-truth partitions in networks

Lena Mangold^{1,2,3,*} and Camille Roth^{1,2,3}

¹*Computational Social Science team, Centre Marc Bloch, Friedrichstr. 191, 10117 Berlin, Germany*

²*Centre national de la recherche scientifique (CNRS), 3 rue Michel-Ange, 75 016 Paris, France*

³*Centre d'Analyse et de Mathématique Sociales (CAMS),*

École des hautes études en sciences sociales (EHESS), 54 Bd Raspail, 75006 Paris, France

(Dated: February 7, 2023)

A myriad of approaches have been proposed to characterise the mesoscale structure of networks – most often as a partition based on patterns variously called communities, blocks, or clusters. Clearly, distinct methods designed to detect different types of patterns may provide a variety of answers to the network’s mesoscale structure. Yet, even multiple runs of a given method can sometimes yield diverse and conflicting results, yielding entire landscapes of partitions which potentially include multiple (locally optimal) mesoscale explanations of the network. Such ambiguity motivates a closer look at the ability of these methods to find multiple qualitatively different ‘ground truth’ partitions in a network. Here, we propose a generative model which allows for two distinct partitions to be built into the mesoscale structure of a single benchmark network. We demonstrate a use case of the benchmark model by appraising the power of stochastic block models (SBMs) to detect coexisting bi-community and core-periphery structures of different strengths. We find that the ability to detect the two partitions individually varies considerably by SBM variant and that coexistence of both partitions is recovered only in a very limited number of cases. Our findings suggest that in most instances only one – in some way dominating – structure can be detected, even in the presence of other partitions in the generated network. They underline the need for considering entire landscapes of partitions when different competing explanations exist and motivate future research to advance partition coexistence detection methods. Our model also contributes to the field of benchmark networks more generally by enabling further exploration of the ability of new and existing methods to detect ambiguity in mesoscale structure of networks.

I. INTRODUCTION

Network structure is frequently characterized at the mesoscale level by the configuration of what is broadly denoted as ‘communities’ — groupings of nodes that display some sort of similarity in terms of their connectivity in the network. Networks may exhibit a wide variety of mesoscale structures, such as densely connected or cohesive clusters, assortative or disassortative communities, core-periphery structures, equivalence classes, or combinations thereof [1, 2]. In turn, there is often more than one scientifically plausible way to divide the nodes of a real-world network, as demonstrated for instance by the coexistence of both cohesive clusters and core-periphery structures in multiple cases [3, 4].

Clearly, methods designed to identify distinct types of mesoscale structures yield different partitions for a given network. Perhaps more remarkably, results produced by different algorithms aimed at identifying one specific type of mesoscale structure may still vary considerably for the same network. A commonly studied empirical example is the Karate Club (KC) network, a friendship network of 34 members of a sports club which split into two new clubs after a fall-out between its members [5]. While the existing literature has repeatedly produced a partition of two cohesive groupings similar in terms of node member-

ship to the division caused by the split of the club [6, 7], variability in what is detected as the ‘optimal’ partition of this network has been demonstrated not only in terms of community membership of nodes [6] but also of the total number of communities recovered [8–10]. Additionally, other types of mesoscale structures can be detected as plausible explanations for the KC network [11], including a core-periphery-type structure of leaders and followers.

Competing explanations of mesoscale structure in real networks, such as the KC example, motivate a further exploration of ambiguity on this scale; perhaps the reason for conflicting results is that multiple qualitatively different ‘ground truths’ and partitions were responsible for the generative process of a network and its mesoscale configuration [12]. In fact, recent work on stochastic block models (SBMs), which have become increasingly popular for mesoscale network description, has emphasised the importance of exploring the variability of the entire partition landscapes that they return, instead of forcing a global consensus from a distribution of partitions (i.e. choosing one among many by maximising some objective) [11]. A further important phenomenon in the context of mesoscale variability is that of detectability limits, where known structures are no longer detected due to lacking signal strength and which have been shown to exist due to the presence of phase transitions in networks generated by SBMs [13, 14].

On the whole, mesoscale variability may thus stem both from the intrinsic ambiguity in the generative processes of the network and from the stochastic ambiguity

* lena.mangold@cmb.hu-berlin.de, she/her/hers

of the generative blockmodel. In this paper we are generally interested in appraising the accuracy of mesoscale structure detection under ambiguity constraints. We choose (1) to start from the KC example as one of the simplest configurations possessing jointly a core-periphery and a bi-community structure, and (2) to rely on SBMs as a theoretical framework accommodating many types of mesoscale structures, beyond clusters and including the two above ones, and that may further be used not only for generating but also for detecting mesoscale structures. More specifically, we are motivated to explore the ability of SBMs to detect certain structures when we *know* that ambiguity exists on the mesoscale. We propose a framework for a generative benchmark model, which can have such ambiguity built into its mesoscale structure by allowing for two qualitatively distinct partitions (i.e. two ‘ground truths’) to be planted into the same network. Using this framework, the two partitions are defined respectively through matrices that specify the connectivity within and between blocks which – similar to the planted partition model [15] – facilitates the analysis of SBMs (or any community detection algorithm) for varying strengths of the planted mesoscale structures. We use our framework to plant two qualitatively different partitions into a synthetic network and try to recover them using two SBM variants. In this way, we analyse the ability of SBMs to detect two competing structures present in a network, appraising both the extent to which each partition is recovered individually as well as the successful detection of the coexistence of both partitions.

This paper is structured as follows. In section II, we provide some background on conflicting explanations of mesoscale structure in networks (II A), the interplay between ambiguity and detectability of block structures (II B), as well as a more general overview of the existing literature on SBMs (II C) and generative benchmark models of mesoscale structures (II D). We then introduce our model framework in section III, covering the derivation of the model in the two-partition case and two variants of generative processes of edge placement in the network. In section IV, we illustrate a use case for our model in form of a set of simulations, the results of which we discuss in section V. We summarise our main results in section VI and briefly touch on possible future work that could extend on our simulations and on the model itself.

II. BACKGROUND

A. Community detection & partition landscapes

Community detection often adopts a clustering perspective and focuses on cohesive communities, which denote groups of nodes more densely connected to other nodes of the same group than to nodes in other groups [16], as opposed to other types of meso-level structures

more generally [2]. Corresponding methods to identify community structure are designed to perform best with specific types of data and networks [12] and many authors have chosen distinct routes to optimise for the most plausible partition (see [17] for a review of different methods). Existing algorithms therefore have at their basis a vast landscape of measures, such as modularity [7], spectral properties [18], generative models [19], betweenness centrality [6], or information-theoretic methods [20], which is only one of the causes for the diversity in results from algorithms that use different approaches.

While the No Free Lunch theorem for community detection — there is no single algorithm that performs best at every community detection task [12] — implies that diversity in approaches is not only helpful but even necessary to solve domain-specific problems in the best possible way, it nevertheless causes a model selection challenge for researchers who lack sufficient domain knowledge. While most community detection algorithms of the 20th century (from cliques to k-cores through CONCOR [21–23]) as well as the Girvan-Newman algorithm [24] popular in the 2000s were deterministic, this challenge has been further exacerbated by the advent of approaches whose results are non-deterministic by nature, such as Louvain [9] and SBM [19, 25, 26]. In that case, even multiple results yielded by one given community detection algorithm may not clearly indicate a consensus partition, leading to a partition selection problem on top of the above-mentioned issue around model selection. In existing work, this has been addressed by finding some kind of consensus in a distribution of partitions to identify an ‘optimal’ partition, for example by averaging over results from multiple runs of the same algorithm [27, 28].

Such consensus-seeking methods run into problems, however, when multiple partitions that are close to the optimum are qualitatively different from each other, uncovering the need for considering multiple local consensus partitions that may provide different, similarly likely explanations to the network structure at hand [11]. The issue of multiple locally optimal partitions was also addressed by Peel *et al.* [12], who demonstrated that many real-world networks have multiple plausible (high likelihood) partitions and that different sets of node meta-data may correlate with different aspects of the structure of the network. These recent results suggest that by accommodating for a diversity of ground truths in the generative process, the stochastic nature of some community detection methods is, in fact, not only an issue to deal with but a feature of these methods.

B. Community detectability & ambiguity

The recent focus on the importance of analysing the variability of partition distributions call for an exploration of what we will call mesoscale ambiguity. In an effort to identify prototypical network partitions representative of various regions of an entire partition landscape

Kirkley and Newman [29] aimed at introducing (and detecting) what they call ‘ambiguity’ on the mesoscale of synthetic networks. By specifying such ambiguity through certain edge probabilities between blocks in an SBM (see section II C for a review of SBMs) they demonstrated the ability of their model to detect a set of representative partitions which identify different aspects of the introduced ambiguity.

This specific example of ambiguity calls for an investigation of the distinction between truly ambiguous block structures on the one hand, and weak or noisy signals which prevent algorithms from correctly detecting mesoscale structures. The stochastically generated SBM ensemble may exhibit some variability in their block structure, but if only one ‘ground truth’ partition is planted, are qualitatively different recovered partitions the result of real ambiguity or merely of detectability issues? And should the detection of partitions which could not have been generated from the planted model (i.e. that lie outside of the distribution of possible networks with the specified parameters) be viewed as a failure of the partitioning algorithm rather than successfully recovered ambiguity?

To distinguish between the correct recovery of ambiguous mesoscale structures and the inability of a community detection algorithm to identify the true partition due to noise that is ‘blurring’ the signal of the block structure, we need to provide some understanding of the detectability phase transitions that have been demonstrated to exist in community detection (see [30] for a review). When the structural signal in a network exists but is too weak or too noisy, it becomes impossible for community detection algorithms to identify such structures. At a certain phase transition, algorithms will mistake a network for a random graph when the structural traces of underlying communities are not sufficiently tangible in the actual network. Prior work on the detectability of modules in network has shown - both analytically as well as heuristically - the existence [31] and positions of such phase transitions, notably for spectral community detection methods [14] and for methods using Bayesian maximum-likelihood [32]. Much of this early work on phase transitions focused on the symmetric case of the traditional (Poisson degree-distributed) SBM. Since then, others have worked on networks with heterogeneous node degree distributions and have argued for the existence of phase transitions in such cases [33] and demonstrated that heterogeneity in networks facilitates the detection of communities in the case of modularity maximisation [34]. While many efforts have gone into the appraisal of phase transitions for community detection for decisive (albeit sometimes noisy) structures, and others have demonstrated that such detectability thresholds do not exist in core-periphery structures [4], little work has focused on the limits of SBMs in truly ambiguous cases. Exploring this further seems particularly important, since the application of community detection methods is primarily aimed at real-world networks, which

arguably exhibit more ‘ambiguity’ and for which the possible existence of multiple locally optimal solutions has been demonstrated repeatedly (see above). As mentioned previously, empirical networks have also been shown to have different types of mesoscale structures all at once - complicating the issue even further.

C. Stochastic block models

In this work, we exploit the features of SBMs two-fold. On the one hand, we use SBMs for *generating* synthetic networks with planted mesoscale structure. On the other hand, we explore the issue of ambiguity in mesoscale structure in networks by fitting SBMs to synthetic graphs and thus using SBMs as a way of *detecting* mesoscale structures. Bayesian inference methods, such as SBMs, are especially suited for the exploration of partition distributions due to their stochastic nature.

SBMs originate in mathematical sociology and were introduced to generate synthetic networks with block structure by configuring an entire distribution over networks with prior characteristics. More precisely, this distribution is defined over a set of networks with the specified number of nodes, block assignments, and within- and between-block edge probabilities [25]. Network generation relies on assigning nodes to blocks and placing edges randomly and independently according to a probability specified by the block membership of each of the two nodes. It is therefore an extension of the simple random graph model, where constant edge probabilities are specific to block pairs rather than being the same for the entire network. An SBM takes as parameters (a) a block membership vector, with entries indicating the block membership of each node, and (b) a connectivity matrix of size equal to the number of blocks, whose elements indicate the probability of a connection between the respective blocks (or within a block for the elements on the diagonal). Since its first appearance, SBMs have been repurposed repeatedly to function as a baseline model for addressing the community detection issue as an inference problem [19, 26, 35]. It is increasingly popular in theoretical and applied network science research, partly due to its flexibility grounded in a relatively general definition of what it means for nodes to be similar i.e., to belong to a block or a community. The idea is that one can ‘reverse’ the generative process of an SBM for the purpose of block structure detection: statistical inference methods can be used to fit SBMs to network data, to recover the parameters of the model (essentially block memberships) that offer the most likely explanation of the generative processes of a network.

Famously, edge placement between two nodes in the ‘traditional’ SBM only depends on the nodes’ block assignment. It therefore does not resemble the structure of many real networks, which tend to have heterogeneous node degree distributions. This issue was addressed by the introduction of ‘degree correction’ into the SBM,

through which edge placements also depends on the respective degree of each node. Using this degree-corrected version as the generative model assumed in the process of detecting block structure considerably improved the ability of SBMs to pick up community structures in real networks [19]. More SBM extensions have since been developed, including hierarchical [36], overlapping [37] and multilayer [38] variants, many of which were demonstrated to be an improvement in the goodness of fit for certain types of networks, compared even to the degree-corrected version. Others have exploited the flexibility of SBMs (in terms of the types of mesoscale structures that can be detected) to demonstrate the diversity of core-periphery structures in real networks [39]. In the existing SBM literature, most work focuses on the recovery of a single partition that is identified by optimising some model selection criterion; however, some recent work has gone beyond the single-partition approach and has emphasised the need to consider the entire partition landscape returned by SBMs [11, 12, 29]. In this work, we intend to contribute to this particular subfield of the SBM literature, by drawing attention to the existence and detectability of more than one planted structure in a single network.

D. Generative benchmark models

As opposed to real-world networks whose exact generative processes are not known, synthetic networks are a natural choice to plant a specific structure and serve as a benchmark, in particular for appraising the success of a certain method in recovering various mesoscale structures, including communities. Such benchmark frameworks allow for certain mesoscale structures to be ‘built into’ a synthetic network, on which the performance of algorithms can be tested by measuring the extent to which the predefined structure is successfully recovered. In general, such benchmarks allow for one or multiple parameters to be adjusted so that the potential limits of an algorithm can be explored by running simulations for varying parameters, and to imitate the features of certain types of real networks. One of the earliest such models is the Girvan-Newman (GN) benchmark [24], which is a network of 128 nodes, divided into four equally-sized groups and relying on one parameter controlling inter-group connectivity strength through the external (out-community) degree of nodes.

To overcome some of its shortcomings, such as its general inflexibility, small size and unrealistic features, Lancichinetti and Fortunato [40] proposed a benchmark accounting for heterogeneous degree and community size distributions. Other existing benchmarks allow for the specification of the within- and between-group connectivity through the use of SBMs, such as the planted partition model [15] which has been extended to other special cases including multilayer networks [41]. In general, the aim of generative benchmark models is to resemble fea-

tures of empirical networks and while many of the existing benchmarks account for one or several such features, the ambiguity in mesoscale structures has as yet been neglected. Our contribution is to focus on this particular aspect and to complement single ground truth benchmarks by a framework that generates networks with multiple built-in ground truths.

III. MODEL FRAMEWORK

We propose a generative network model whose parameters aim to simultaneously respect two partitions: edges are placed between node pairs in a way such that the resulting network exhibits a block structure that takes into account each of these two partitions at the same time. As stated above, we are generally guided by the KC example where both a bi-community and a core-periphery structure may be found and where it is likely that the two structures jointly explain the network formation.

A. Formal outline

We generate a network with N nodes and M edges, into which we plant a set of $S = 2$ partitions. Edges between nodes are described by the adjacency matrix $\mathbf{Y} \in \mathbb{R}^{N \times N}$. We focus on the undirected, unweighted case, whereby $Y_{ij} = Y_{ji} = 1$ if i and j are connected by an edge and 0 otherwise.

In each partition s , we plant K_s blocks into the network structure; in this two-partition case, we choose $K_s = K_1 = K_2 = 2$ blocks. \mathfrak{B}_s denotes the set of block labels in partition s so that $|\mathfrak{B}_s| = K_s = 2$. Specifically, we choose $\mathfrak{B}_1 = \{a, b\}$ and $\mathfrak{B}_2 = \{c, d\}$. Since nodes simultaneously ‘exist’ in these different partitions, each node i is assigned to exactly one block in each partition. The block structure in each partition s is defined by (1) the block membership vector $\boldsymbol{\pi}_s$, where $\pi_{s_i} \in \mathfrak{B}_s$ denotes the block membership of node i in partition s , and (2) the edge density matrix $\boldsymbol{\theta}_s$ of size $K_s \times K_s$, where diagonal (resp. off-diagonal) elements indicate the density of within-block (resp. between-block) edges. Using the block membership distribution of nodes in $\boldsymbol{\pi}_s$, it is straightforward to deduce the edge count matrix \mathbf{B}_s (also of size $K_s \times K_s$), which has as its elements the average *number* of edges within and between blocks.

The simultaneous block membership of nodes in two partitions means that each node is assigned a combination of blocks across the $S = 2$ partitions and we denote the set of possible such combinations by $\boldsymbol{\Gamma} = \mathfrak{B}_1 \times \mathfrak{B}_2 = \{(a, c), (a, d), (b, c), (b, d)\}$. This means that we can rephrase our problem as follows: To plant multiple partitions in one single network, we generate a network in which we plant one *single* partition with K blocks, where $K = |\boldsymbol{\Gamma}| = |\mathfrak{B}_1| |\mathfrak{B}_2| = 4$. We call this partition the *cross-partition* and the $K = 4$ new blocks the *cross-blocks*. We index the elements of the set of

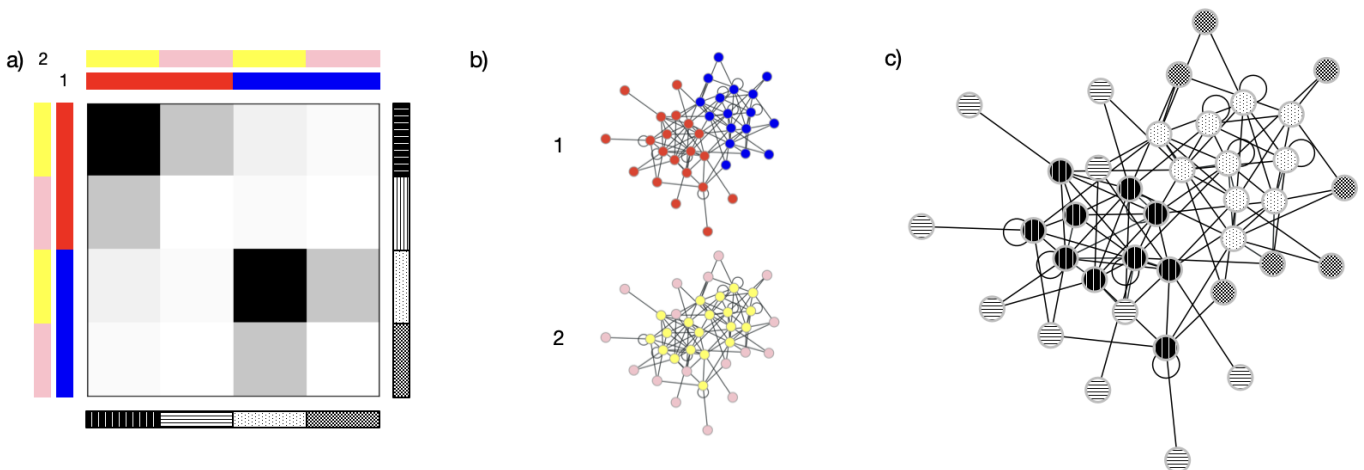


FIG. 1: Connectivity matrix (a) with coloured and pattern-filled bars showing the two planted partitions (left and top) and the resulting cross-partition (right and bottom). Generated networks, with nodes coloured according to two planted partitions (b) and resulting cross-partition (c).

cross-block labels Γ from 1 to 4, so that $\Gamma = \{\Gamma_j\}$ for $j \in \{1, 2, 3, 4\}$. For each node i in our network, we create a block membership one-hot vector $\mathbf{z}_i \in \mathbb{R}^K$ to indicate which of the $K = 4$ cross-blocks i belongs to. Specifically, if i is in cross-block $\Gamma_j \in \Gamma$ then the j 's element of \mathbf{z}_i is equal to 1.

Our generative network then simply becomes a standard SBM where the probability of an edge between two nodes i and j is determined entirely by the probability of a node between the cross-block u of i and the cross-block v of node j . To generate the final network, we therefore need to determine the connectivity between and within the K cross-blocks. Similar to the edge density matrix $\boldsymbol{\theta}_s$ and edge count matrix \mathbf{B}_s for each planted partition s , we will need $\boldsymbol{\theta}$ and \mathbf{B} . As above, element θ_{uv} denotes the probability of an edge between cross-blocks u and v and B_{uv} denotes the average number of such edges. The connectivity matrices are created in a way in which the probabilities of edges between cross-blocks satisfy the edge count matrices \mathbf{B}_s for each planted partition s .

Note that the notion of overlapping blocks (i.e. the assignment of nodes to multiple blocks at the same time) reminds of the mixed membership stochastic block model (MMSBM) [42]. The central distinction lies in the way in which nodes occupy multiple blocks simultaneously. In MMSBM, nodes are associated with each block with a certain probability, denoted by a probability vector; in our case – since a node exists at the same time in each of the S partitions and is assigned to one of K_s blocks in each partition s – nodes belong to multiple such blocks with equal probability.

The schematic in Figure 1 illustrates the coexistence of two partitions in a single cross-partition: the coloured bars on the top and left of the block matrix in (a) illustrate the blocks to which nodes belong in the two planted partitions visualised in (b); the patterned bars on the right and bottom of the matrix represent the cross-block

membership as visualised in (c). Note that the schematic illustrates the specific case of a planted bi-community structure coexisting with a core-periphery structure. In this schematic, we denote the community structure ‘partition 1’ and the core-periphery structure ‘partition 2’, which is how the two planted structures are labelled in the schematic. In section III B we present the derivation of the connectivity matrices which incorporate two potentially qualitatively different planted partitions.

We plant two partitions in the form of the matrices in Eqs. (1a) and (1b), where the elements denote the edge densities within and between blocks. The matrices are symmetric since the graphs we are generating are undirected (for example $p_{ab} = p_{ba}$) and – according to convention in undirected networks and to simplify calculations later – elements on diagonals denote twice the within-block edge densities.

$$\begin{cases} \boldsymbol{\theta}_1 = \begin{pmatrix} p_{aa} & p_{ab} \\ p_{ab} & p_{bb} \end{pmatrix} & (1a) \\ \boldsymbol{\theta}_2 = \begin{pmatrix} q_{cc} & q_{cd} \\ q_{cd} & q_{dd} \end{pmatrix} & (1b) \end{cases}$$

B. Cross-block matrix: equal block sizes

In the first instance, we focus on the case of equal block sizes, both in the planted partitions as well as the cross-partition. We fix all blocks to have n nodes i.e., $2n = N$. We allow for self-loops, so we have $\mathbf{B}_1 = n^2 \boldsymbol{\theta}_1$ and $\mathbf{B}_2 = n^2 \boldsymbol{\theta}_2$. We denote the vector of block sizes in the cross-partition by $\boldsymbol{\nu} = (\nu_{ac}, \nu_{ad}, \nu_{bc}, \nu_{bd})$ and constrain cross-blocks to be equally-sized: $\nu_i = \nu$ for $i \in \Gamma$ and thus $2\nu = n$. We discuss the more general case of varying block and cross-block sizes in section III C.

We create the symmetric $K \times K$ matrix $\hat{\boldsymbol{\theta}}$, whose elements are the products of the elements of $\boldsymbol{\theta}_1$ and $\boldsymbol{\theta}_2$

corresponding to the respective blocks in 1 and 2 that make up the cross-blocks in $\mathbf{\Gamma}$. Matrix $\hat{\theta}$ is thus the Kronecker product of θ_1 and θ_2 , where the order depends on the index set J ,

$$\hat{\theta} = \theta_1 \otimes \theta_2 = \begin{matrix} & \begin{matrix} (a, c) & (a, d) & (b, c) & (b, d) \end{matrix} \\ \begin{matrix} (a, c) \\ (a, d) \\ (b, c) \\ (b, d) \end{matrix} & \begin{pmatrix} p_{aa}q_{cc} & p_{aa}q_{cd} & p_{ab}q_{cc} & p_{ab}q_{cd} \\ p_{aa}q_{cd} & p_{aa}q_{dd} & p_{ab}q_{cd} & p_{ab}q_{dd} \\ p_{ab}q_{cc} & p_{ab}q_{cd} & p_{bb}q_{cc} & p_{bb}q_{cd} \\ p_{ab}q_{cd} & p_{ab}q_{dd} & p_{bb}q_{cd} & p_{bb}q_{dd} \end{pmatrix} \end{matrix} \quad (2)$$

The edge count matrix in this case is denoted by $\mathbf{B} = \nu^2 \theta = \nu^2 x \hat{\theta}$, where x is chosen in such a way that the number of edges within and between certain block pairs in \mathbf{B} add up to the respective elements of \mathbf{B}_1 and \mathbf{B}_2 . For example, the average number of edges within and between blocks (a, c) and (a, d) (the sum of the elements of the upper left 2×2 sub-matrix of \mathbf{B}) needs to be equal to $p_{aa}n^2$, the average number of edges within block a in partition 1. Choosing x in this way, we mechanically satisfy the requirement that the sum of all elements of \mathbf{B} is $2M$. For our simple case, this holds for $x = \frac{4}{\sum_{ij} \theta_{1,ij}} = \frac{4}{\sum_{ij} \theta_{2,ij}}$ (see Appendix A for the derivation).

C. Cross-block matrix: the general case

In any other more general case in terms of varying block sizes, a constant x satisfying both planted partitions only exists if we introduce other constraints. For example, if we keep $2n = N$ but allow for varying cross-block sizes in \mathbf{B} , we have $\nu_1 = \nu_{ac} = \nu_{bd}$ and $\nu_2 = \nu_{ad} = \nu_{bc}$; in this case, we can find a constant x for which \mathbf{B} satisfies both planted partitions and $\nu_1 \neq \nu_2$ if we have the trivial case of $p_{aa} = p_{ab} = p_{bb}$ and $q_{cc} = q_{cd} = q_{dd}$ i.e., we are planting a random graph (see Appendix B).

When this does not hold, and for more general cases in which each block in partitions 1 and 2 can take on any size, we need to determine a symmetric $K \times K$ matrix of multiplicative factors $\mathbf{X} = \{x_{ij}\}$ to create the final edge density matrix $\theta = \mathbf{X} \circ \hat{\theta}$, where \circ denotes the element-wise multiplication of the two matrices. Here, the maximum number of edges between and within each block – both in the two planted partitions as well as the cross-partition – may differ for each block pair. The edge count matrices are therefore $\mathbf{B}_s = \mathbf{n}_s \mathbf{n}_s^T \circ \theta_s$ for $s \in \{1, 2\}$, where \mathbf{n}_s is the vector of block sizes in planted partition s , and $\mathbf{B} = \nu \nu^T \circ \theta = \nu \nu^T \circ \mathbf{X} \circ \hat{\theta}$, where ν is the vector of cross-block sizes.

Finding the elements of \mathbf{X} in the general, undirected case for $K_s = K_1 = K_2 = 2$ and $K = 4$ can be formulated as a system of equations with $2 \times \frac{K_s(K_s+1)}{2} = 6$ equations and $\frac{K(K+1)}{2} = 10$ unknowns. Since this system of equations is underdetermined there is no unique solution; instead we can compute the minimum norm solution, which is unique and always exists if any solution

to the system exists (see Appendix C). While we use the specific equal-block case for our simulations in section IV, we have shown here that a more general set-up is also possible.

D. Generative SBM

We generate the final network from the connectivity matrices according to the ‘traditional’ SBM [25], which uses matrix θ alongside cross-block membership vectors \mathbf{z} to determine whether or not an edge exists between two nodes. More specifically, we will place an edge between each pair of nodes (i, j) independently at random, with probability θ_{uv} , where $u, v \in \mathbf{\Gamma}$ are the cross-blocks of i and j respectively. We thus sample the value of the interaction between i and j with $Y_{ij} \sim \text{Bernoulli}(\mathbf{z}_i^T \theta \mathbf{z}_j)$. In this version of the SBM, edge counts in \mathbf{B} are satisfied on average.

We also consider the microcanonical SBM [26], in which the (rounded) elements of the given edge count matrix \mathbf{B} are satisfied exactly (rather than on average) and which is based on the configuration model [43]. Specifically, we consider the degree-corrected extension of this microcanonical SBM, in which the probability of an edge being placed between two nodes does not depend solely on the elements of a connectivity matrix but also on a given degree sequence or distribution. This SBM variant has been demonstrated to have characteristics that more closely resemble empirical networks, by producing synthetic networks with the type of within-block degree variability that is more likely to occur in real networks [19]. Given a degree sequence \mathbf{k} in which k_i denotes the degree of node i , this works by assigning k_i half-edges to node i and then choosing two half-edges in the network at random (allowing for self-edges) and connecting them under the condition that the given within- and between-block edge counts are satisfied. However, the elements of edge count matrix \mathbf{B} can be real numbers and must therefore be rounded in the network generation process. This introduces small differences between the (planted) edge count matrices \mathbf{B}_s and the generated networks in terms of the total number of edges as well as the within- and between- cross-block edge counts. It also means that a given degree sequence can only be satisfied exactly if $\mathbf{B} \in \mathbb{Z}^{N \times N}$; in our simulations we sample node degrees from a power law distribution rather than satisfying the exact degree sequence. Note that in the graphs we generate in this way in our simulations below, any pair of nodes is connected by a maximum of one unweighted edge; removing this constraint and producing multigraphs instead is straightforward.

The version of our model which generates networks according to the traditional SBM will from now on be called the *canonical model* to distinguish it from the latter version, which we will call the *microcanonical model*. This is to avoid confusion in the notation between the SBM variants we use to *generate* our networks from those we

use to infer partitions.

IV. SIMULATIONS

We now explore the extent to which multiple built-in ground truths are recovered by SBMs by generating a set of networks in which we plant two partitions. Clearly, there are many interesting two-partition structures one may explore. As indicated before, we are interested in the type of structure present in our motivating example, the KC network. For this network, samples of the posterior distribution of inferred partitions yield a number of plausible explanations of the mesoscale structure [11]; one local consensus partition is the famous two-faction division of the network into two assortative communities, another is a leader-follower partition that resembles a core-periphery structure. We are interested in the recovery limits of these two types of structures in networks and we therefore plant similar structures into an ensemble of synthetic networks according to our generative framework. In our simulations, we build both a bi-community as well as core-periphery structure into a set of graphs and we fit two different SBM variants to our networks to infer the posterior distribution of partitions for each of them. We finally calculate the similarity between the recovered partitions and the planted partitions and present the results for the partitions planted by each model variant and recovered by each SBM variant.

A. Parameters

We focus on the case of equal block sizes here, for which the multiplicative factor x is a constant and we do not have to rely on the minimum norm solution (see section III B). We plant networks with $N = 400$ and we run three sets of simulations with varying average degree $\langle k \rangle = 5; 10; 20$. Nodes are chosen uniformly at random and assigned to each block to create block membership vectors $\boldsymbol{\pi}_1$ and $\boldsymbol{\pi}_2$. To plant the two partitions, we must also define edge count matrices \mathbf{B}_1 and \mathbf{B}_2 . Partition 1 (\mathbf{B}_1) configures the bi-community structure whereby a parameter μ controls intra- vs. inter-block connectivity strength. Partition 2 (\mathbf{B}_2) configures the core-periphery (CP) partition, in which the edge density within the core and the edge density among peripheral nodes is controlled by parameter λ . We use the edge count matrix in (3a) to plant two equally-sized communities and (3b) to plant a core-periphery structure.

$$\begin{cases} \mathbf{B}_1 = M \begin{pmatrix} 1 - \mu & \mu \\ \mu & 1 - \mu \end{pmatrix} \\ \mathbf{B}_2 = M \begin{pmatrix} 1 - \lambda & \frac{1}{2} \\ \frac{1}{2} & \lambda \end{pmatrix} \end{cases} \quad (3a) \quad (3b)$$

We use our model to generate multiple sets of networks, sweeping parameters μ and λ from 0.01 to 0.5 at incre-

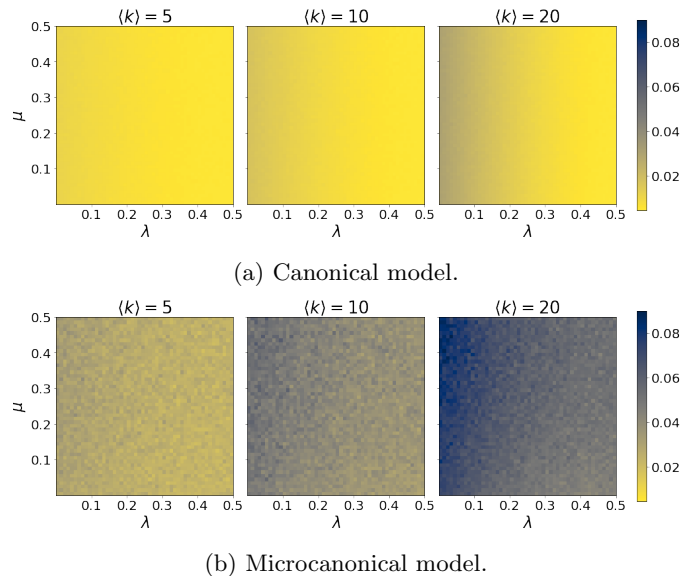


FIG. 2: Mean normalised degree variance for graphs with varying average degrees $\langle k \rangle$.

ments of 0.01 in each case. Note that we exclude $\mu = 0$ as it would yield a disconnected graph of two components and exclude $\lambda = 0$ for symmetry in the two dimensions.

Low values of μ generate assortative community structure (in the sense that most edges are placed within blocks and few between blocks), while μ close to 0.5 produce a network close to a random graph. Values of λ close to zero generate ‘clear’ core-periphery structure, with most edges being placed within the core and few among peripheral nodes, while $\lambda = 0.5$ produces a random graph.

B. Generated graphs

To appraise differences in degree distributions, we use the canonical model in one set of simulations and the microcanonical model in another. We thus generate two sets of networks for each average degree $\langle k \rangle$. In the canonical model, node degrees follow a Poisson degree distribution and edge counts within and between blocks are satisfied on average. In the microcanonical case, as described in section III D, edge counts do not fluctuate across different runs of the model and we impose further constraints on the node degrees, which we sample from a power law distribution with exponent $\gamma = 3$. We use a soft constraint, in the sense that the final network does not have to match the given degree sequence exactly, but only on average. See Appendix D for a summary of the small deviations of the edge counts in the generated graphs from the planted edge count matrices due to rounding errors. In both cases, we generate 8 networks for each (λ, μ) -pair, to account for possible fluctuations in the generative process.

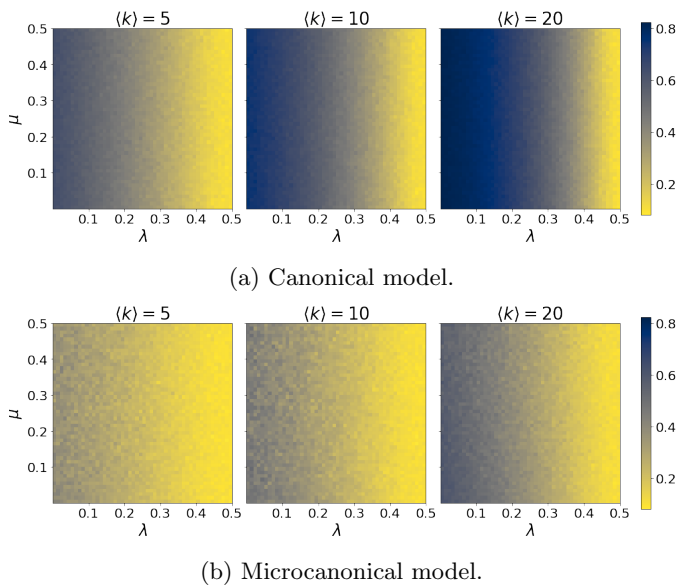


FIG. 3: Mean Jensen-Shannon distance between core and periphery node degree distributions for graphs with varying average degrees $\langle k \rangle$.

Before attempting to recover planted partitions in the two sets of graphs, we explore structural characteristics introduced into the networks for different (λ, μ) -pairs and through the two different generative processes of the canonical and microcanonical model. Figure 2 demonstrates that, unsurprisingly, degree variance is highest across the entire (λ, μ) space for graphs generated by the microcanonical model, since we sample a heterogeneous powerlaw degree distribution. It is considerably lower for graphs generated by the canonical version. Notwithstanding, using the canonical model, higher degree heterogeneity is introduced into networks for lower values of λ , for which we are imposing a strong core-periphery structure (see Figure 8 in the appendix for a rescaled version of the top row of Figure 2).

While graphs produced by the microcanonical model exhibit the highest degree heterogeneity overall, Figure 3 illustrates that their core and periphery blocks are more similar in terms of node degree distributions than in the canonical case, measured by the Jensen-Shannon distance [44] between the degree distributions of the core nodes and those of the peripheral nodes. In the canonical case, node degrees are Poisson distributed for the network as a whole, as well as for nodes within each block. However, to accommodate for the core-periphery structure, the mean of the distribution is lower in the periphery than in the core, which in the Poisson case leads to a relatively small overlap between the two distributions [4]. In the microcanonical case, we introduce degree heterogeneity through the degree distribution so that planting CP structures does not produce the same differences in the block degree distributions.

This means that were we to simply assign nodes with

above average degree to the core and those with below average degree to the periphery in graphs generated by the canonical model we would retrieve more correctly assigned nodes than in networks produced by the microcanonical model [4], where by ‘correctly’ we refer to the CP block planted by \mathbf{B}_2 as defined in (3b). The heterogeneity in degree distributions in the microcanonical case may generate other types of core-periphery patterns than the planted ones. (See Appendix D for a comparison of the number of correctly classified nodes in this way for the two models and of the degree distributions of the core and the periphery nodes for two example graphs.)

It is thus worth elaborating on the potential consequences of specifying the degree distribution as an extra parameter in the generative process in particular, additionally to the planted connectivity matrix and block assignments of nodes. While we expect the graphs produced by the canonical model to exhibit structure closely related to what we explicitly plant (i.e. the block connectivity matrices), we may implicitly be introducing additional structure through the constraints imposed on node degrees in the microcanonical case. Heterogeneity in degree distributions, for example, may lead to groups of nodes that display similarities in their connectivity with the rest of the network in terms of their number of connections; it is possible that the dividing lines between these groups do not correspond with those imposed by our planted block structure, which may lead to structures other than those explicitly planted being picked up. These differences in degree heterogeneity introduced through the generative process are thus likely to have an impact on the extent to which SBM variants recover the (coexistence of the) planted partitions in different regions of the (λ, μ) plane, as is confirmed in section V.

C. Similarity measure

To quantify the similarity between planted and recovered partitions, we calculate the partition overlap $\omega(x, y)$, namely the proportion of nodes in one partition x assigned to the same, assumed correct, block of the other partition y [11]. This is calculated by finding the bijection $x' = \zeta(y)$ of the group labels of y , so that the number of nodes that have the same block label in x' and x is maximised, so that we have

$$\omega(x, y) = \frac{1}{N} \max_{\zeta} \sum_i \delta_{x_i, \zeta(y_i)}. \quad (4)$$

Specifically, this is done by solving the maximum weighted bipartite matching problem for two partitions using a function from the `graph_tool` python library [45], which is based on the Kuhn-Munkres [46, 47] algorithm. Note that here we use the normalised version, which is between 0 and 1. Therefore, $\omega = 1$ when all nodes of two partitions coincide. Note that in the two-block case, $\omega = 0.5$ implies that half of the nodes are classified correctly and therefore the two partitions are not correlated.

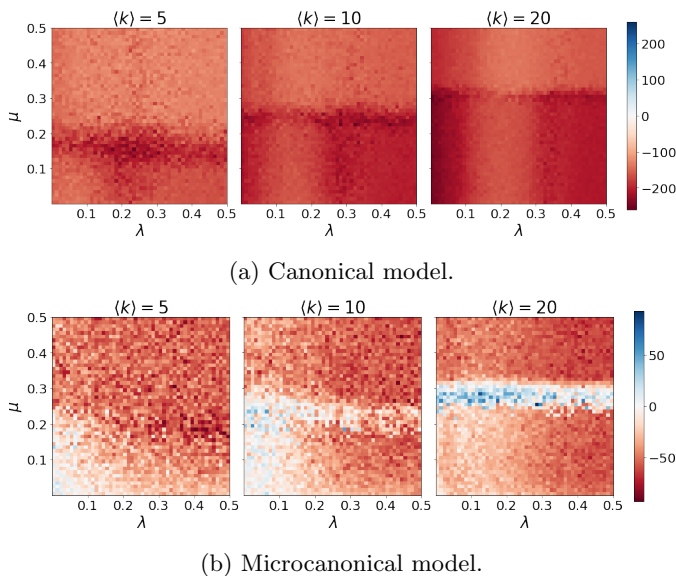


FIG. 4: Difference between the log-evidence of the DC and NDC model class for graphs with varying average degrees $\langle k \rangle$. Negative values (red) indicate a better fit of the NDC model, positive values (blue) indicate a better fit of the DC model.

V. RESULTS

To infer partitions of the generated graphs, we fit two SBM variants (traditional and degree-corrected) using the ‘graph_tool’ python library [45]. We retrieve a distribution of 50 partitions for each graph and therefore a total of 400 partitions for each combination of μ and λ . In its function as an inference method, we from now refer to the traditional SBM as NDC (non-degree-corrected SBM) and to the degree-corrected variant as DC, to avoid confusion with the models (canonical and microcanonical) used to generate our networks. We finally calculate the partition overlap ω between inferred partitions and planted partitions for the two planted structures as well as between the inferred partitions and the planted cross-partition.

A. Model fit

We start by evaluating which of the two SBM variants used for the detection of mesoscale structures provides a better fit to our generated networks. We calculate the (log) model evidence, summed over all partitions for each run, calculated by subtracting the entropy of the posterior distribution from the negative average description length (over all partitions) [26]. Figure 4a demonstrates that for the canonical version NDC is the preferred model across the entire (λ, μ) space; this is unsurprising as edge placement in the generative process is independent of node degree. When we use the microcanonical version

(in which we *do* take into account the node degrees in the generative process), we may have expected DC to be a better description of the generated networks across the entire (λ, μ) plane. However, Figure 4b demonstrates that this is not the case: we observe a small region of λ and μ values for which DC has the larger model evidence; for increasing average degree, this region becomes more pronounced and exists across the entire λ range, while restricted to more and more narrow values of μ . Everywhere else, NDC still provides a better model fit. This suggests that the higher complexity of DC is justified only for networks with a high level of heterogeneity in the degree distribution *and* bi-community structure of a certain strength which depends on $\langle k \rangle$. It seems that – in terms of the number of model parameters – DC provides an overly complex description everywhere else in the (λ, μ) plane, although degree heterogeneity is still high.¹

B. Recovery of each planted structure

In Figure 5, we show the mean partition overlap for all partitions in the posterior distribution of inferred partitions for each (λ, μ) pair, for networks generated by two models. Remember that partition 1 refers to the bi-community structure and partition 2 refers to the core-periphery structure.

We first focus on the partitions inferred from the graphs generated by the canonical model, where node degrees follow Poisson distributions. In Figure 5a, we show the mean partition overlap $\langle \omega \rangle$ between planted partitions and those recovered by NDC (on the left-hand side) and DC (on the right-hand side).

Both variants detect the bi-community structure frequently up to a certain threshold value of μ , which increases for higher $\langle k \rangle$. It turns out that the locations of the thresholds are roughly in line with what is described in existing literature on detectability thresholds for the planted partition model [13, 14]. According to this work, community structure planted by edge count matrix \mathbf{B}_1 as defined in (3a) is detectable for $\langle k \rangle > \frac{1}{(1-2\mu)^2}$; in our case this should place our threshold μ_T for detectability at $\mu_T \approx 0.276$ ($\langle k \rangle = 5$), $\mu_T \approx 0.342$ ($\langle k \rangle = 10$), and $\mu_T \approx 0.388$ ($\langle k \rangle = 20$). In our simulations, both variants detect bi-communities up to a similar value μ , which is slightly below μ_T . We observe a second type of threshold for bi-community detection, this time along the λ dimension. For low values of λ , both variants fail to detect the

¹ If we allow for multiple edges between node pairs (using the graph_tool python library [45]), we find an additional area in the bottom-left of the (λ, μ) plane – roughly for values $\lambda < 0.2$ and $\mu < 0.33$ – in which DC is preferred. A possible explanation could be the larger degree variance introduced in this case, for which the higher complexity of DC is justified. As the partition recovery patterns for these multigraphs are equivalent to the ones we discuss in section V, we restrict our analysis to simple graphs.

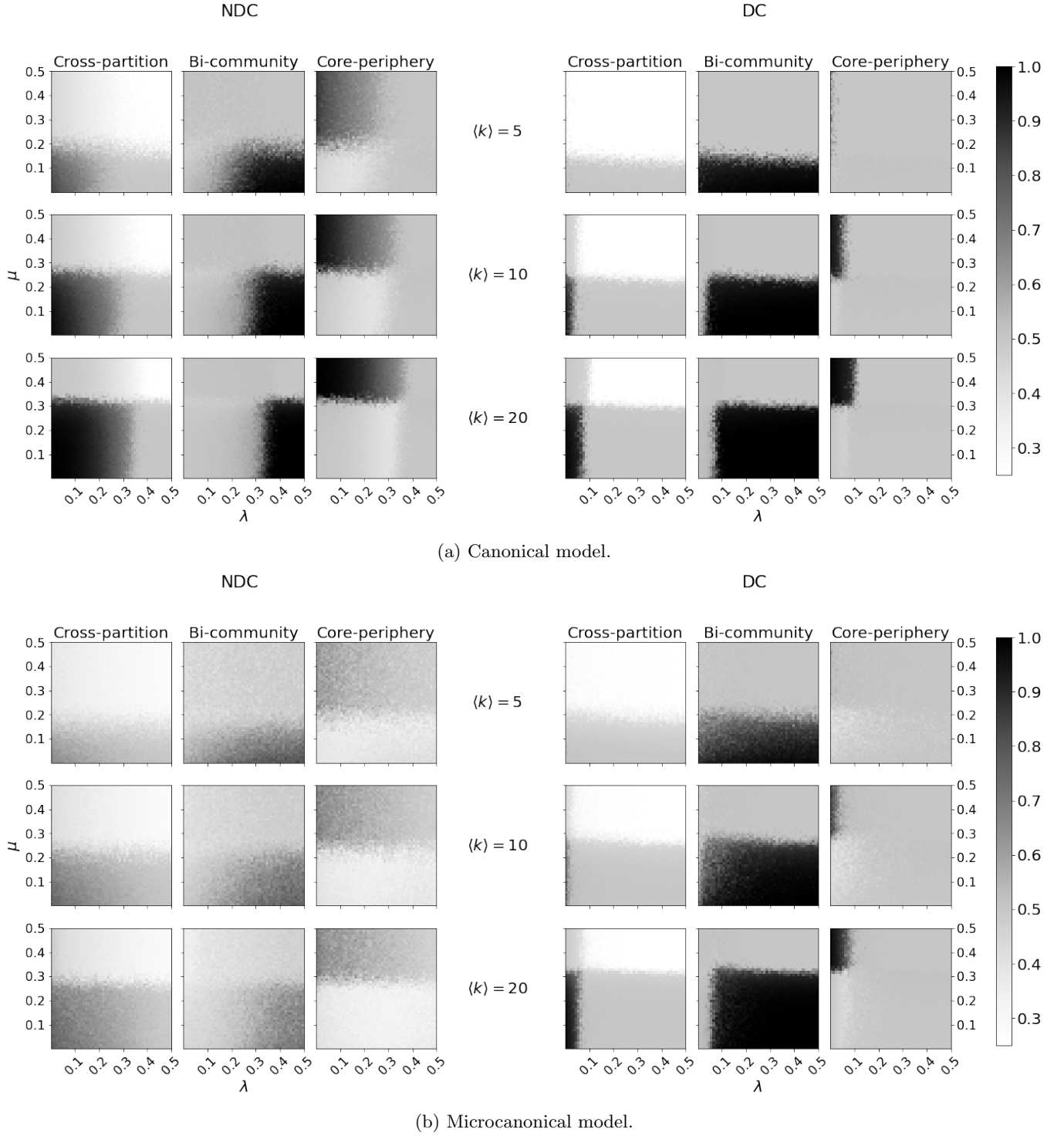


FIG. 5: Mean partition overlap $\langle \omega \rangle$ between the planted partitions and the partitions in the posterior distributions for the assortative community structure (partition 1) and the core-periphery structure (partition 2) for graphs with varying average degrees $\langle k \rangle$.

bi-community partition even though $\mu < \mu_T$ and they appear to uncover the cross-partition instead. While the threshold along the μ dimension is similar for NDC and DC, we find that the λ threshold is much higher for NDC

than for DC. This means that NDC recovers the cross-partition up to higher values of λ than DC, after which bi-communities are detected. The λ threshold also increases with growing $\langle k \rangle$.

The detection of the planted core-periphery partition also depends on the average degree of the networks. In fact, the thresholds of CP detection correspond with those described above for bi-community detection: along the μ dimension, CP structure is detected once cross-partitions and bi-communities are no longer recovered; along the λ axis, CP structure is detected until its structure is too weak, at which point bi-communities are detected. This is somewhat contradictory to the work by Zhang *et al.* [4], who find no evidence for a detectability threshold in the case of core-periphery structures.

One of the main differences between NDC and DC in the canonical case is therefore the thresholds at which structures do and do not get detected along the λ axis. For all values of $\langle k \rangle$ and for both SBM variants, the cross-partition is recovered when the bi-community and CP structures are strong. Along each direction, both variants then start picking up the respective bi-block structure once the signal becomes weaker. Since both the bi-community and CP structures are only recovered when the signal for the respective other structure is weak, the coexistence of both structures in the inferred partition distribution is rare; we revisit this in section V D. As both thresholds (along λ and μ) are higher for larger $\langle k \rangle$, the cross-partition detection region increases for denser graphs; this phenomenon is more pronounced for NDC, which provides a better model fit than DC across the entire (λ, μ) plane.

C. Influence of degree distribution

To explore the influence of a heterogeneous degree distribution on partition recovery, we fit the two SBM variants to a set of networks generated by the microcanonical model. Figure 5b illustrates the mean recovery of partitions in this case by NDC (left) and DC (right). The overall detection patterns resemble those discussed for the canonical case. For DC, all partitions are recovered in similar regions with similar thresholds, albeit slightly more ‘fuzzy’ boundaries on said thresholds. However, we observe a substantial difference in the performance of the NDC variant, for which the $\langle \omega \rangle$ is considerably lower for all planted partition across the entire (λ, μ) plane. In the first instance, this is somewhat surprising, since we have seen in section V A that even for graphs generated by the microcanonical version NDC provides a better description. A plausible explanation of this phenomenon is the additional structural features that we introduce through the extra constraint on node degrees in our microcanonical model and the thereby imposed degree heterogeneity (see section IV B). It turns out that for relatively strong bi-community structures, the NDC variant recovers layered CP structures within each of the two community blocks, both for very strong planted CP structures but also when no explicit CP structure is planted at all (see example graphs in Appendix F). When CP structures are planted explicitly with strong signal, the layered CP par-

tion recovered by NDC bears some resemblance to the cross-partition; when no explicit CP structure is planted, the layered CP structures within two assortative blocks resemble more the bi-community partition (according to ω and upon visual inspection of the example networks). As can be seen in Figure 5b, the DC variant detects partitions much closer to the planted cross-partition (for lower λ) and the bi-community (for higher λ) value than NDC. However, the NDC variant has the better model fit; this implies that by forcing heterogeneous degrees, we may to some extent be ‘overfeeding’ more structure into the network than solely that defined through the block connectivity matrices.

D. Recovery of structure coexistence

Other than the individual recovery of the two planted partitions, we are naturally also interested in the appearance of both structures in different regions of the partition landscape detected in a given network, that we denote as *coexistence*. Specifically, we want to know whether the posterior distribution of partitions inferred by SBM features both planted partitions (rather than only one or the other) for any particular set of (λ, μ) pairs. We measure coexistence recovery by setting the threshold for the partition overlap to $\omega_T = 0.75$, for which we consider an inferred partition to be close enough to the planted partition to be considered a ‘successful recovery’.

To illustrate the coexistence detection, we plot the fraction $\alpha = \frac{P_1}{P_1+P_2}$, where P_1 denotes the proportion of partitions in the posterior distribution that resemble the bi-community partition, given ω_T , and P_2 denotes the equivalent for CP partitions. The results for each model/variant combination are shown in Figure 6. For $\alpha = 1$ (dark blue) we only detect the bi-community structure, for $\alpha = 0$ (dark red) only the CP structure is present in the posterior distribution, and values close to $\alpha = 0.5$ (white) indicate a more balanced posterior distribution, which features both partitions to some extent; such values are found where the detection areas for the two planted partitions appear to be touching or even overlapping. The grey region represents (λ, μ) pairs for which α is undefined since neither of the two structures is recovered successfully.

We observe in Figure 6c that – as expected from the results in section V C – fitting NDC to graphs generated by the microcanonical model does not yield partition distributions anywhere in our (λ, μ) -space that feature both bi-community *and* CP partitions. In all other cases, there are small regions for which coexistence is detected, for this relatively generous threshold value of $\omega_T = 0.75$. Note that for more generous ω_T thresholds, we observe reduced recovery regions for each partition in all cases and therefore an even smaller or completely absent region of overlap in which both partitions feature in a given posterior distribution (see Appendix E).

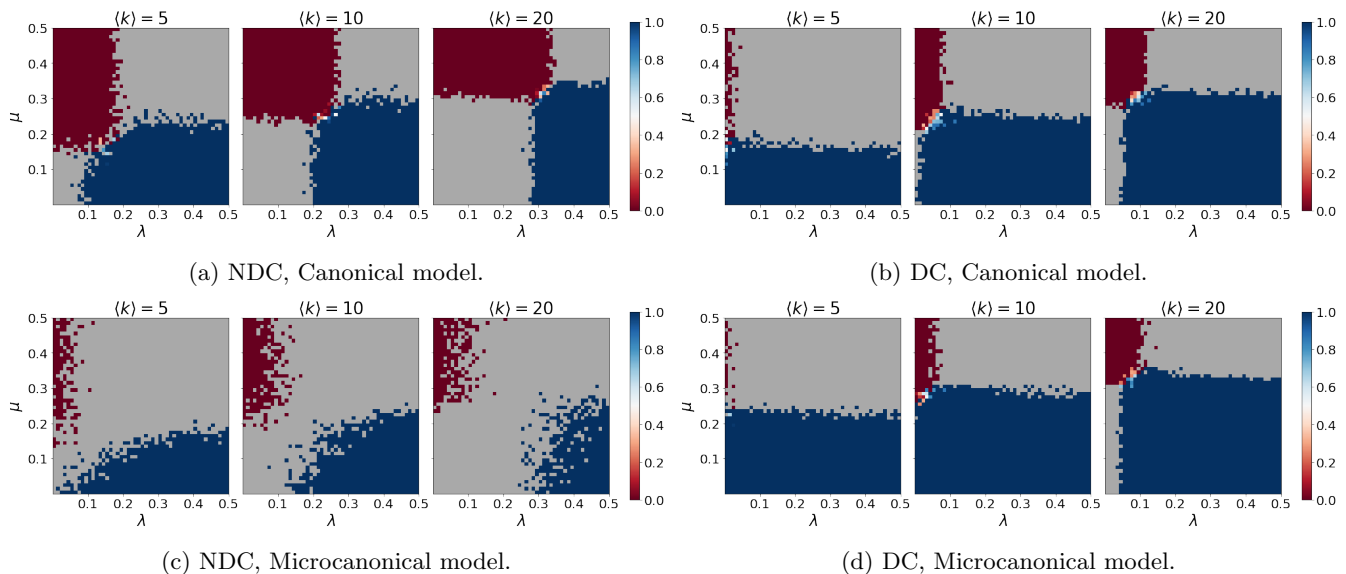


FIG. 6: Fraction α of recovered bi-community partitions out of all successfully recovered partitions for varying average degrees $\langle k \rangle$ for $\omega = 0.75$; at $\alpha = 1$ (resp. $\alpha = 0$) only the bi-community (resp. CP) structure is detected.

E. Discussion

Overall, we found detectability thresholds for each individual planted structure and we discovered that coexistence of the two structures is only detected in a very small number of cases. We also observed considerable differences in successful partition recovery between the NDC and DC variants, which are more pronounced when they are fitted to graphs generated by the microcanonical model than when fitted to those produced by the canonical version.

We briefly discuss the effect of degree heterogeneity introduced into networks through the generative process of the microcanonical model. We found that, by constraining the degree distributions in this way, we are inadvertently introducing CP divisions *beyond* the explicitly planted CP structure. The additional CP structures are picked up by NDC since it does not correct for node degrees and it thus comparatively ‘underperforms’ at detecting individual planted partitions and coexistence of multiple partitions. These findings are consistent with existing SBM literature, including the original work in which the degree-corrected variant was introduced [19]. They should serve as a reminder that a network may exhibit multiple conflated structural properties which could in turn complicate the detection of certain types of partitions or even lead to the detection of spurious mesoscale structures. In general, and specifically if previous knowledge exists about structural properties that are likely to be present in a network (e.g., high degree variance) or about certain types of structures that are of interest, one should consider carefully the SBM variant that is appropriate. Methods which specifically aim to disentangle conflated structural properties [19, 48] or to recover cer-

tain types of structures, such as assortative communities [49], could be considered.

Secondly, we focus on the canonical model and the extent to which the two SBM variants recover the bi-community and CP partitions relative to each other, jointly (coexisting in a given posterior distribution) and relative to the cross-partition. Overall, we have found that thresholds for the detection of the individual planted partitions and for the detection of structure coexistence depend on the average degree of a network as well as the SBM variant used to detect the structure. The NDC variant – which has higher model evidence – does better at picking up the cross-partition at the expense of recovery of the CP structure. It recovers coexistence of bi-community and CP partitions to a slightly lesser extent than DC. Since we are *explicitly* planting the cross-partition, and only *implicitly* planting the bi-community and CP structures by making sure the edge probabilities within and between the respective cross-blocks satisfy those within and between the blocks of the two bi-block partitions, it is perhaps not surprising that the variant with the better model fit is the one that favours the cross-partition at the cost of coexistence detection.

Irrespective of whether we use NDC or DC, we find that even in this relatively simple case of planting only two qualitatively different ground-truth partitions, the region in our structural strength landscape for which the coexistence of the bi-community and CP structures is detected is limited to an extremely small area. This is concerning since mesoscale structures in real networks are unlikely to be so simple and a larger number of coexisting network partitions and a multitude of different structures may be present. Clearly, more research is necessary to better understand whether the lack of coexis-

tence recovery is due to a detectability limit after which it is impossible for any algorithm to detect coexistence (similar to the known community detection detectability threshold [13, 14]), or whether some other SBM variant would be able to do a better job at detecting coexistence of multiple planted structures. More work should then also focus on expanding the relatively recent literature on partition diversity [11, 29] by advancing existing methods or developing new tools. The aim should be to enable researchers to reliably explore multiple coexisting ground truth partitions that may have been responsible for the generation of a given network, which we suspect to be the case in real graphs [12]. In this sense, our framework and findings should be seen as a benchmark against which new SBM variants developed for this purpose can be tested. Such models should then at least pass the test of expanding the region shown in Figure 6.

More generally, the fact that even for existing methods coexistence *is* detected in certain regions of our structural strength landscape emphasises again the importance of acknowledging the diversity and possible dissensus in partition distributions, and for more researchers in the field of applied network science to consider multiple plausible explanations of the mesoscale of network.

VI. CONCLUSION

We have proposed a framework for generative network models that exhibit predefined ambiguity in their mesoscale structure. This framework complements existing generative networks as a *two-ground-truth benchmark* that can be used to measure the extent to which mesoscale structure detection algorithms recover the ambiguity introduced by two simultaneously planted partitions. We found that the coexistence of two qualitatively different partitions (bi-community and core-periphery structure) is only detected in a very small region in our ‘structural strength’ space, which varies in size and shape for different versions of our model and for different SBM variants used for mesoscale structure detection. Only when both structures are sufficiently strong and neither dominates the other can we recover the existence of both. In the majority of cases, each of the two planted partitions is recovered when the strength of the other structure is weak. We have thus uncovered a type of detectability threshold in the case where multiple types of mesoscale structures influence the network construction. Since the coexistence of more than one plausible explanation for mesoscale structures appears to be a common phenomenon in real networks [12], we believe that exposing the presence of such an – as of yet understudied – detectability threshold is an important contribution to the SBM literature, especially as most community detection approaches still aim at uncovering a single partition and at validating it against a single ground truth. More work is required to explore the nature of these detectability thresholds analytically, and to appraise detectability

limits exhibited by other types of coexisting structures, for example including more than one community partition or bipartite structures; the combination of certain types of structures may be more or less prone to detectability issues than others, especially given the ability (or lack) of certain SBM variants to detect certain types of structures. We conclude that future work around the theory of methods for mesoscale structure detection in networks should focus on improving existing methods to be able to identify coexisting structures. More broadly, and in line with recent work [11, 29], we believe that researchers applying existing methods on real networks should focus on the possibility of discovering multiple dimensions of segmenting the network, rather than accepting unidimensional solutions, that may be even be averaged over ‘multimodal’ partition distributions. In particular, possible contexts in which considering multiple plausible network divisions seem particularly important include the sub-field of computational social science which deals with the analysis of interaction dynamics in online public spaces. Appraising the coexistence of multiple types of structures in social media interaction networks, such as community/CP structures or even qualitatively different community partitions (maybe generated through non-aligned political dimensions, as has been recently shown on Twitter affiliations [50]), could have considerable benefits for researching online conversation dynamics. In this context, researchers should consider the coexistence of qualitatively different structures and be mindful of the detectability issues addressed here. In our simulations, we focus on the special case of equally sized blocks in both the planted partitions as well as the cross-partition and on the community-CP case. However, the benchmark model is flexible to a diverse range of structures of varying block sizes, degree distributions, and planted mesoscale structures. Future work may use this benchmark to analyse the recovery of ambiguity in networks of different sizes and average degrees or with other combinations of mesoscale structures. This work may also be extended by testing other types of detection algorithms (beyond SBM) on this benchmark model. Further extensions of the benchmark model itself could allow for more than two blocks in each planted partition, more than two planted partitions or a directed version of the model.

ACKNOWLEDGMENTS

This work was supported by the “Socsemics” Consolidator grant from the European Research Council (ERC) under the European Union’s Horizon 2020 research and innovation program (grant agreement No. 772743).

Appendix A: Constant multiplicative factor

The most general form of defining the multiplicative factor is the symmetric matrix \mathbf{X} of size $K \times K$, such that $\mathbf{B} = \mathbf{X} \circ \nu \nu^T \circ \hat{\boldsymbol{\theta}}$. If we fix $\nu = \frac{n}{2}$ for all blocks in Γ (and allow for self-loops) we have that the maximum number of edges between and within each group is $\nu^2 = \frac{n^2}{4}$ and therefore $\nu \nu^T = \nu^2 \mathbf{1}\mathbf{1}^T$, so

$$\mathbf{B} = \nu^2 \mathbf{X} \circ \hat{\boldsymbol{\theta}} = \nu^2 \mathbf{X} \circ \begin{pmatrix} p_{aa} \begin{pmatrix} q_{cc} & q_{cd} \\ q_{cd} & q_{dd} \end{pmatrix} & p_{ab} \begin{pmatrix} q_{cc} & q_{cd} \\ q_{cd} & q_{dd} \end{pmatrix} \\ p_{ab} \begin{pmatrix} q_{cc} & q_{cd} \\ q_{cd} & q_{dd} \end{pmatrix} & p_{bb} \begin{pmatrix} q_{cc} & q_{cd} \\ q_{cd} & q_{dd} \end{pmatrix} \end{pmatrix}. \quad (\text{A1})$$

We want to find multiplicative factors, such that the sum of the elements of the upper left 2×2 block matrix of \mathbf{B} is equal to $B_1[1,1]$, and so on for the the diagonal and upper triangular elements of \mathbf{B}_1 . Seeing equation (A1) alongside

$$\mathbf{B}_1 = n^2 \boldsymbol{\theta}_1 = n^2 \begin{pmatrix} p_{aa} & p_{ab} \\ p_{ab} & p_{bb} \end{pmatrix} \quad (\text{A2})$$

it is clear that we can find a constant x , such that $\mathbf{X} = x \mathbf{1}\mathbf{1}^T$, for which the sum of the elements of each non-overlapping 2×2 block matrix of \mathbf{B} is equal to the corresponding element in \mathbf{B}_1 . Clearly this also works for \mathbf{B}_2 , if we rewrite equation (A1) with the reverse order of the Kronecker product, $\hat{\boldsymbol{\theta}}' = \boldsymbol{\theta}_2 \otimes \boldsymbol{\theta}_1$,

$$\mathbf{B}' = \nu^2 \mathbf{X} \circ \begin{pmatrix} q_{cc} \begin{pmatrix} p_{aa} & p_{ab} \\ p_{ab} & p_{bb} \end{pmatrix} & q_{cd} \begin{pmatrix} p_{aa} & p_{ab} \\ p_{ab} & p_{bb} \end{pmatrix} \\ q_{cd} \begin{pmatrix} p_{aa} & p_{ab} \\ p_{ab} & p_{bb} \end{pmatrix} & q_{dd} \begin{pmatrix} p_{aa} & p_{ab} \\ p_{ab} & p_{bb} \end{pmatrix} \end{pmatrix} \quad (\text{A3})$$

and for comparison

$$\mathbf{B}_2 = n^2 \boldsymbol{\theta}_2 = n^2 \begin{pmatrix} q_{cc} & q_{cd} \\ q_{cd} & q_{dd} \end{pmatrix}. \quad (\text{A4})$$

For such a constant x we have $\mathbf{B} = \nu^2 x \hat{\boldsymbol{\theta}}$; writing this out for the within-block edges of the original block a , we have

$$p_{aa} n^2 = \nu^2 x \sum_{\substack{i \in \{1,2\}, \\ j \in \{1,2\}}} \hat{\theta}_{ij} = p_{aa} x \frac{n^2}{4} \sum_{ij} \theta_{2ij}. \quad (\text{A5})$$

and similarly for all other elements (on the diagonal and upper triangular) of \mathbf{B}_1 and \mathbf{B}_2 . Equation (A5) gives

$$x = \frac{4}{\sum_{ij} \theta_{1ij}} = \frac{4}{\sum_{ij} \theta_{2ij}}, \quad (\text{A6})$$

where the second equality holds because the sum of the elements of $\boldsymbol{\theta}_1$ and $\boldsymbol{\theta}_2$ must be equal by definition.

With this multiplicative factor we can therefore create our matrices $\boldsymbol{\theta}$ and \mathbf{B}

$$\boldsymbol{\theta} = x \hat{\boldsymbol{\theta}} \quad (\text{A7})$$

$$\mathbf{B} = \nu^2 \boldsymbol{\theta} \quad (\text{A8})$$

Appendix B: Varying block sizes

In the case of equal block sizes in \mathbf{B}_1 and \mathbf{B}_2 but allowing for varying block sizes in \mathbf{B} , we can write $\nu_1 = \nu_{ac} = \nu_{bd}$ and $\nu_2 = \nu_{ad} = \nu_{bc}$, where ν_{ac} is the number of nodes in block (a, c) . In this case, we have $\nu_1 + \nu_2 = n$. We no longer have the same maximum number of edges within and between each of the block pairs, since $\boldsymbol{\nu} = (\nu_1, \nu_2, \nu_2, \nu_1)$. Therefore, instead of (A1), we have

$$\mathbf{B} = \mathbf{X} \circ \nu \nu^T \circ \begin{pmatrix} p_{aa} \begin{pmatrix} q_{cc} & q_{cd} \\ q_{cd} & q_{dd} \end{pmatrix} & p_{ab} \begin{pmatrix} q_{cc} & q_{cd} \\ q_{cd} & q_{dd} \end{pmatrix} \\ p_{ab} \begin{pmatrix} q_{cc} & q_{cd} \\ q_{cd} & q_{dd} \end{pmatrix} & p_{bb} \begin{pmatrix} q_{cc} & q_{cd} \\ q_{cd} & q_{dd} \end{pmatrix} \end{pmatrix}. \quad (\text{B1})$$

with

$$\nu \nu^T = \begin{pmatrix} \nu_1^2 & \nu_1 \nu_2 & \nu_1 \nu_2 & \nu_1^2 \\ \nu_1 \nu_2 & \nu_2^2 & \nu_2^2 & \nu_1 \nu_2 \\ \nu_1 \nu_2 & \nu_2^2 & \nu_2^2 & \nu_1 \nu_2 \\ \nu_1^2 & \nu_1 \nu_2 & \nu_1 \nu_2 & \nu_1^2 \end{pmatrix} \quad (\text{B2})$$

Let us assume that a constant x , such that $\mathbf{X} = x \mathbf{1}\mathbf{1}^T$, does exist for $n = \frac{N}{2}$, $\nu_1 \neq \nu_2$ and that we are planting non-trivial partitions where the probability of edge placement between blocks is not uniform across block pairs. For such an x , the sums of the 2×2 block matrices of \mathbf{B} are equal to the corresponding elements of \mathbf{B}_1 (and the sum of the block matrices of \mathbf{B}' are equal to the elements of \mathbf{B}_2). We can then write the equations for \mathbf{B}_1 as

$$p_{aa} n^2 = x p_{aa} (q_{cc} \nu_1^2 + q_{dd} \nu_2^2 + 2q_{cd} \nu_1 \nu_2) \quad (\text{B3a})$$

$$p_{ab} n^2 = x p_{ab} (q_{cd} \nu_1^2 + q_{cd} \nu_2^2 + q_{cc} \nu_1 \nu_2 + q_{dd} \nu_1 \nu_2) \quad (\text{B3b})$$

$$p_{bb} n^2 = x p_{bb} (q_{dd} \nu_1^2 + q_{cc} \nu_2^2 + 2q_{cd} \nu_1 \nu_2). \quad (\text{B3c})$$

This means that

$$q_{cc} \nu_1^2 + q_{dd} \nu_2^2 + 2q_{cd} \nu_1 \nu_2 = q_{dd} \nu_1^2 + q_{cc} \nu_2^2 + 2q_{cd} \nu_1 \nu_2$$

$$(q_{cc} - q_{dd})(\nu_1^2 - \nu_2^2) = 0. \quad (\text{B4a})$$

$$(\text{B4b})$$

Since $\nu_1 \neq \nu_2$, we have $q_{cc} = q_{dd}$ and therefore (from equations (B3a) and (B3b)), we then have

$$q_{cc} \nu_1^2 + q_{cc} \nu_2^2 + 2q_{cd} \nu_1 \nu_2 = q_{cd} \nu_1^2 + q_{cd} \nu_2^2 + 2q_{cc} \nu_1 \nu_2$$

$$(q_{cc} - q_{cd})(\nu_1 - \nu_2)^2 = 0, \quad (\text{B5a})$$

$$(\text{B5b})$$

and hence $q_{cc} = q_{cd} = q_{dd}$. Clearly, taking the same steps for \mathbf{B}_2 gives $p_{aa} = p_{ab} = p_{bb}$. This is a contradiction to our set of assumptions and therefore such a constant x does not exist (apart from the trivial case where we plant a random graph).

Appendix C: Solving underdetermined system of equations

For the most general case in which we allow both the sizes and densities to vary between the blocks in \mathbf{B}_1 and \mathbf{B}_2 , we need to determine the elements of multiplicative factor matrix \mathbf{X} . The elements (on the diagonal and upper triangular) of this matrix need to be chosen in such a way that the elements of \mathbf{B}_1 and \mathbf{B}_2 are satisfied, as is presented in equations (C1a) to (C1f). Here $b_{aa} = n_{aa}\theta_{aa} = B_1[1, 1]$ and we have dropped the subscripts for partitions 1 and 2 for legibility. Subscripts on the right-hand side are written as the matrix indices of \mathbf{X} and $\hat{\mathbf{B}}$; element x_{11} , for example, is short for x_{aacc} and denotes the multiplicative factor for within-block edges in block (a, c) (overlap of block a in s_1 and block c in s_2).

$$\begin{cases} b_{aa} = x_{11}\hat{B}_{11} + 2x_{12}\hat{B}_{12} + x_{22}\hat{B}_{22} & \text{(C1a)} \\ b_{ab} = x_{13}\hat{B}_{13} + x_{14}\hat{B}_{14} + x_{23}\hat{B}_{23} + x_{24}\hat{B}_{24} & \text{(C1b)} \\ b_{bb} = x_{33}\hat{B}_{33} + 2x_{34}\hat{B}_{34} + x_{44}\hat{B}_{44} & \text{(C1c)} \\ b_{cc} = x_{11}\hat{B}_{11} + 2x_{13}\hat{B}_{13} + x_{33}\hat{B}_{33} & \text{(C1d)} \\ b_{cd} = x_{12}\hat{B}_{12} + x_{14}\hat{B}_{14} + x_{32}\hat{B}_{32} + x_{34}\hat{B}_{34} & \text{(C1e)} \\ b_{dd} = x_{22}\hat{B}_{22} + 2x_{24}\hat{B}_{24} + x_{44}\hat{B}_{44}. & \text{(C1f)} \end{cases}$$

Equations (C1a) to (C1f) are an underdetermined system of six linear equations with ten unknowns (all elements of \mathbf{X} on the diagonal and upper triangle). We can write it in matrix form as

$$\mathbf{A}\mathbf{x} = \mathbf{b} \quad \text{(C2)}$$

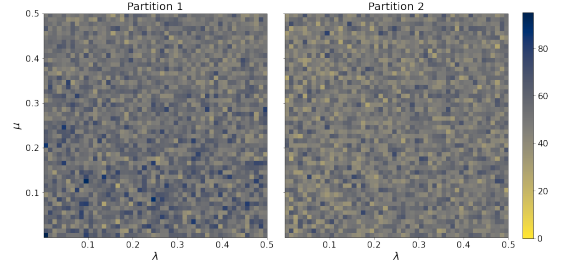
with

$$\mathbf{x} = (x_{11}, x_{12}, \dots, x_{32}, x_{33}, x_{44}) \quad \text{(C3)}$$

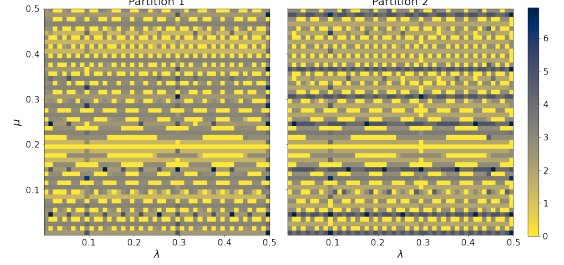
$$\mathbf{b} = (b_{aa}, b_{ab}, b_{bb}, b_{cc}, b_{cd}, b_{dd}) \quad \text{(C4)}$$

so that $\mathbf{x} \in \mathbb{R}^{10}$, $\mathbf{b} \in \mathbb{R}^6$ and where $\mathbf{A} = \{a_{ij}\} \in \mathbb{R}^{6 \times 10}$ is the coefficient matrix with elements of $\hat{\mathbf{B}}$ respecting equations (C1a)-(C1f). According to the Rouché–Capelli theorem, we know that such an underdetermined system has an infinite number of solutions if and only if the rank of its coefficient matrix is equal to the rank of its augmented matrix $\mathbf{W} = [\mathbf{A}|\mathbf{b}] \in \mathbb{R}^{6 \times 11}$. This is always true for two well-defined connectivity matrices \mathbf{B}_1 and \mathbf{B}_2 ; clearly, the total number of edges must be the same in the two planted partitions, and we can show that $\text{rank}(\mathbf{A}) = \text{rank}(\mathbf{W})$ if and only if $b_{aa} + b_{ab} + b_{bb} = b_{cc} + b_{cd} + b_{dd}$.

In general, an underdetermined linear system $\mathbf{A}\mathbf{x} = \mathbf{b}$ with $\mathbf{A} \in \mathbb{R}^{m \times n}$ where $m < n$, does not have a unique solution \mathbf{x} . Since the system is underconstrained, it has an infinitude of solutions, if it has any solutions at all. A popular method for solving under- (or over-) constrained systems of linear systems of equations is called *least squares* method. The idea behind the least squares method is to find a solution \mathbf{x} which minimises the squared Euclidean norm of the residual $r(\mathbf{x}) = \mathbf{b} - \mathbf{A}\mathbf{x}$. In other words, we want to find \mathbf{x} that minimises $\phi(\mathbf{x}) =$



(a) Canonical model.



(b) Microcanonical model.

FIG. 7: Mean difference (Frobenius norm) between planted and generated edge count matrices in networks.

$\|r(\mathbf{x})\|_2^2 = \|\mathbf{b} - \mathbf{A}\mathbf{x}\|_2^2$, which can be done by obtaining \mathbf{x} such that $\nabla\phi(\mathbf{x}) = 0$. From this, we obtain the so-called *normal equations* $\mathbf{A}^T\mathbf{A}\mathbf{x} = \mathbf{A}^T\mathbf{b}$ which can be solved analytically if $\mathbf{A}^T\mathbf{A}$ is invertible. In our case, $\mathbf{A}^T\mathbf{A} \in \mathbb{R}^{n \times n}$ has rank at most m , where $m < n$, and is therefore singular. This means that – in this underdetermined case – the normal equations cannot be solved analytically. Instead, we can find the particular least squares solution that minimises the Euclidean norm $\|\mathbf{x}\|_2$ (or its square) with the constraint $\mathbf{A}\mathbf{x} = \mathbf{b}$. When there are no other constraints, this *minimum norm solution* $\hat{\mathbf{x}}$ can be found by computing the singular value decomposition (SVD) in order to compute the Moore–Penrose pseudoinverse \mathbf{A}^+ of matrix \mathbf{A} . The minimum norm solution can then be calculated as $\hat{\mathbf{x}} = \mathbf{A}^+\mathbf{b}$, always exists and is unique [51].

Appendix D: Characteristics of generated graphs

To ensure that the variability in the recovered partitions is not in fact due to the graphs we generate, we compare the planted edge count matrices \mathbf{B}_1 and \mathbf{B}_2 with the actual edge counts in the generated graphs, \mathbf{M}_1 and \mathbf{M}_2 by calculating $\|\mathbf{B}_1 - \mathbf{M}_1\|_F$ and $\|\mathbf{B}_2 - \mathbf{M}_2\|_F$ for all values of μ and λ . Figure 7a shows the mean Frobenius norm for $\mu \in [0.01, 0.5]$ and $\lambda \in [0.01, 0.5]$ for graphs generated by the canonical model. Figure 7b shows the same plot for the microcanonical SBM. These figures show the distances for graphs with average degree $\langle k \rangle = 5$; we note that the patterns for the higher values of $\langle k \rangle$ are similar. We observe that the distances between the planted and generated edge count matrices in the microcanonical case

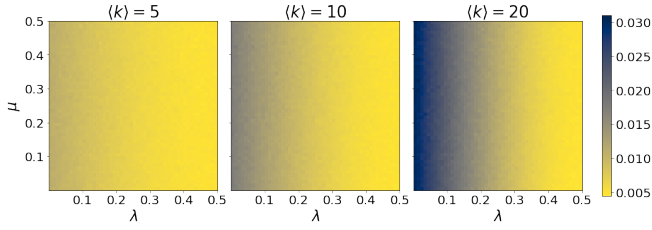


FIG. 8: Mean normalised degree variance for graphs with varying average degrees $\langle k \rangle$, only showing the graphs generated by the canonical model to illustrate the degree variance introduced for low values of λ .

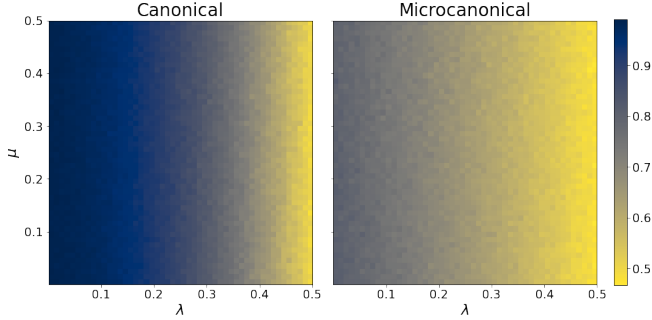


FIG. 9: Proportion of nodes correctly classified into core and periphery blocks by assigning nodes with degree higher than the average degree $\langle k \rangle = 20$ to the core and all others to the periphery.

are – by definition – much lower than in the traditional case. The non-random patterns we observe in the microcanonical case are due to rounding that is necessary to create the edge count matrix \mathbf{B} which is used to generate networks in this case (while in the canonical case the edge probabilities – rather than counts – are used).

Figure 8 shows the rescaled version of Figure 2 in the main text. Here, we plot the mean normalised degree variance for graphs generated by the canonical model, to illustrate the higher variance introduced for lower values

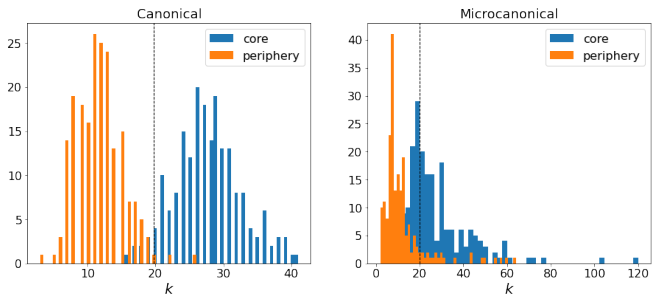
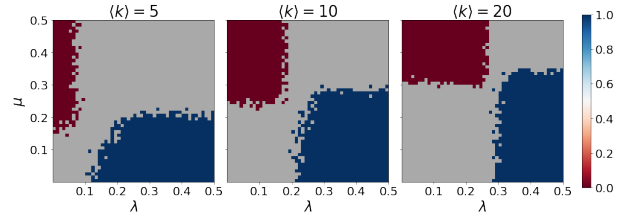
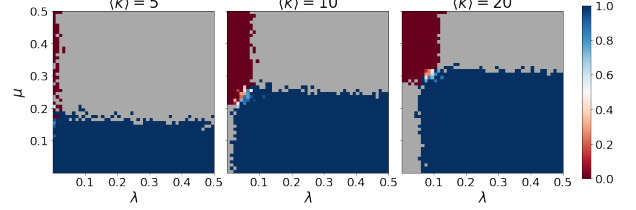


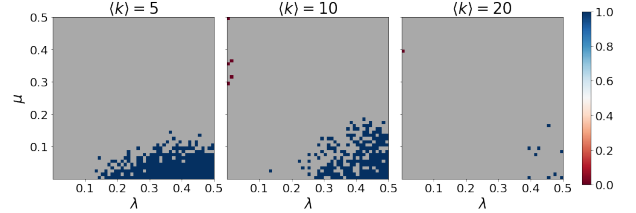
FIG. 10: Degree distributions of core nodes vs periphery nodes in the canonical and microcanonical model with overall average degree (dashed line), for $\mu = 0.1$, $\lambda = 0.1$ and $\langle k \rangle = 20$



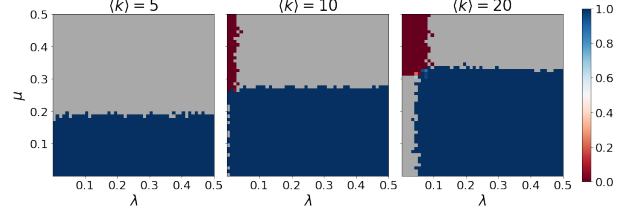
(a) NDC, Canonical model.



(b) DC, Canonical model.



(c) NDC, Microcanonical model.



(d) DC, Microcanonical model.

FIG. 11: Fraction α of recovered bi-community partitions out of all successfully recovered partitions for varying $\langle k \rangle$ for $\omega = 0.85$; at $\alpha = 1$ (resp. $\alpha = 0$) only the bi-community (resp. CP) structure is detected.

of λ , especially for higher values of $\langle k \rangle$.

In Figure 9, we plot the proportion of nodes correctly classified (according to the planted core and periphery blocks) by assigning nodes with above average degree to the core and those with below average degree to the periphery, for graphs with average degree $\langle k \rangle = 20$. In Figure 10, we show two example degree distributions for $\mu = 0.1$, $\lambda = 0.1$ and $\langle k \rangle = 20$.

Appendix E: Stricter partition-overlap thresholds

Figure 11 and Figure 12 illustrate the detection of the bi-community and CP structures, as well as their coexistence, for the two SBM variants and for partition overlap $\omega = 0.85$ and $\omega = 0.95$ respectively.

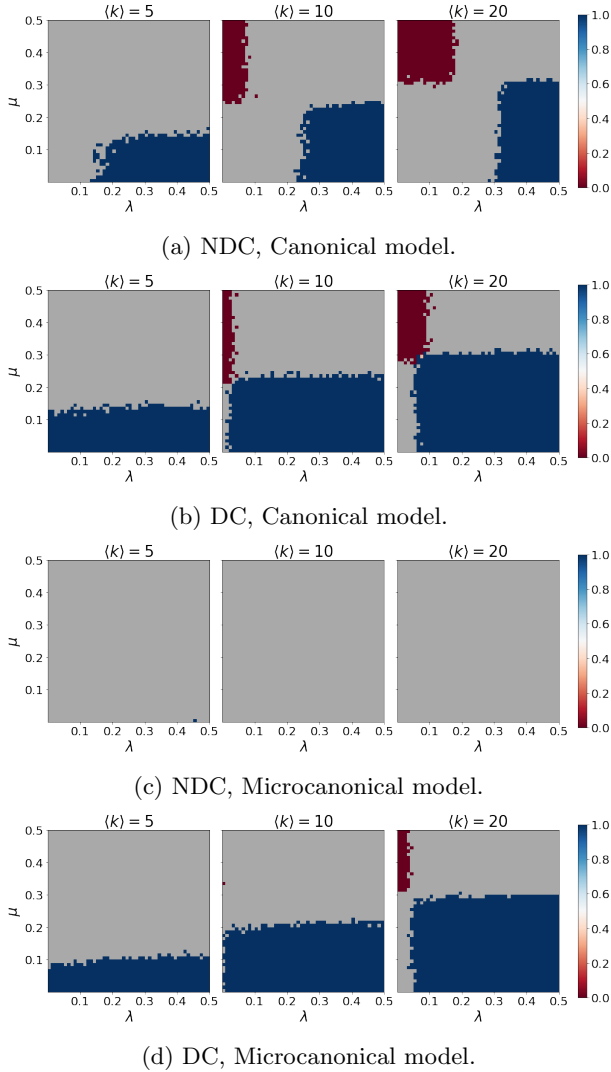


FIG. 12: Fraction α of recovered bi-community partitions out of all successfully recovered partitions for varying $\langle k \rangle$ for $\omega = 0.95$; at $\alpha = 1$ (resp. $\alpha = 0$) only the bi-community (resp. CP) structure is detected.

Appendix F: Example networks with high degree heterogeneity

In Figure 13, we plot two example networks generated by the microcanonical model. The network visualisations were generated by the graph_tool python library [45]. We fix $\mu = 0.1$ for both networks and we create one graph with a strong planted CP structure ($\lambda = 0.01$) and one for which no CP structure at all is planted explicitly through the edge count matrices ($\lambda = 0.5$). Figure 13a and Figure 13c show an example of the type of partition frequently recovered by NDC for $\lambda = 0.01$ and $\lambda = 0.5$ respectively. Figure 13b and Figure 13d show the same but for the DC variant. We observe that DC recovers the cross-partition for $\lambda = 0.01$ and the bi-community partition for $\lambda = 0.5$, in line with the equivalent results

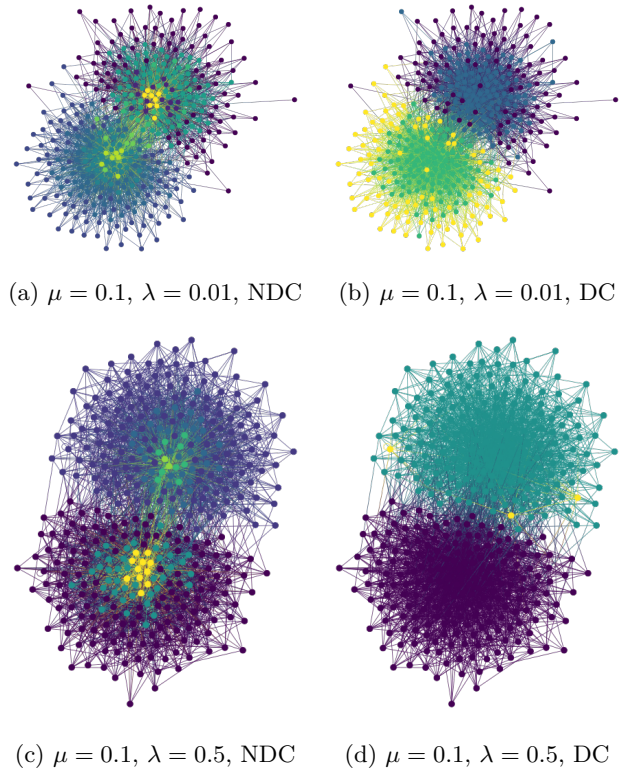


FIG. 13: Example networks for a fixed value of $\mu = 0.1$ and varying value of $\lambda = 0.01; 0.5$.

for graphs generated by the microcanonical model and with what we explicitly planted. NDC, however, (which has higher model evidence) detects a similar structure for $\lambda = 0.01$ and $\lambda = 0.5$: a two-block partition, where each block contains a core and multiple layered peripheries. The difference between the two detected partitions is the number of layers in the core-periphery structures within each block and the size of the outer periphery. Due to these differences, the partition detected for $\lambda = 0.01$ is more similar to the cross-partition, while that detected for $\lambda = 0.5$ is more similar to the bi-community partition.

-
- [1] J. Leskovec, K. J. Lang, A. Dasgupta, and M. W. Mahoney, *Internet Mathematics* **6**, 29 (2009).
- [2] M. Rosvall, J.-C. Delvenne, M. T. Schaub, and R. Lambiotte, in *Advances in Network Clustering and Blockmodelling* (John Wiley & Sons, Ltd, 2019) Chap. 4, pp. 105–119.
- [3] P. Rombach, M. A. Porter, J. H. Fowler, and P. J. Mucha, *SIAM Review* **59**, 619 (2017).
- [4] X. Zhang, T. Martin, and M. E. J. Newman, *Physical Review E* **91**, 032803 (2015).
- [5] W. W. Zachary, *Journal of Anthropological Research* **33**, 452 (1977).
- [6] M. E. J. Newman and M. Girvan, *Physical Review E* **69**, 026113 (2004).
- [7] M. E. J. Newman, *Proceedings of the National Academy of Sciences* **103**, 8577 (2006).
- [8] J. Duch and A. Arenas, *Physical Review E* **72**, 027104 (2005).
- [9] V. D. Blondel, J.-L. Guillaume, R. Lambiotte, and E. Lefebvre, *Journal of Statistical Mechanics: Theory and Experiment* **2008**, P10008 (2008).
- [10] T. S. Evans, *Journal of Statistical Mechanics: Theory and Experiment* **2010**, P12037 (2010).
- [11] T. P. Peixoto, *Physical Review X* **11**, 021003 (2021).
- [12] L. Peel, D. B. Larremore, and A. Clauset, *Science Advances* **3**, e1602548 (2017).
- [13] A. Decelle, F. Krzakala, C. Moore, and L. Zdeborová, *Physical Review E* **84**, 066106 (2011).
- [14] A. Decelle, F. Krzakala, C. Moore, and L. Zdeborová, *Physical Review Letters* **107**, 065701 (2011).
- [15] A. Condon and R. M. Karp, *Random Structures & Algorithms* **18**, 116 (2001).
- [16] R. D. Alba, *Journal of Mathematical Sociology* **3**, 113 (1973).
- [17] S. Fortunato, *Physics Reports* **486**, 75 (2010).
- [18] M. E. J. Newman, *Physical Review E* **88**, 042822 (2013).
- [19] B. Karrer and M. E. J. Newman, *Physical Review E* **83**, 016107 (2011).
- [20] M. Rosvall and C. T. Bergstrom, *Proceedings of the National Academy of Sciences* **105**, 1118 (2008).
- [21] R. D. Luce and A. D. Perry, *Psychometrika* **14**, 95 (1949).
- [22] S. B. Seidman, *Social networks* **5**, 269 (1983).
- [23] R. L. Breiger, S. A. Boorman, and P. Arabie, *Journal of mathematical psychology* **12**, 328 (1975).
- [24] M. Girvan and M. E. Newman, *Proceedings of the national academy of sciences* **99**, 7821 (2002).
- [25] P. W. Holland, K. B. Laskey, and S. Leinhardt, *Social Networks* **5**, 109 (1983).
- [26] T. P. Peixoto, *Physical Review E* **95**, 012317 (2017).
- [27] A. Lancichinetti and S. Fortunato, *Scientific reports* **2**, 1 (2012).
- [28] A. Tandon, A. Albeshri, V. Thayananthan, W. Alhalabi, and S. Fortunato, *Physical Review E* **99**, 042301 (2019).
- [29] A. Kirkley and M. E. J. Newman, *Communications Physics* **5**, 1 (2022).
- [30] C. Moore, *The Computer Science and Physics of Community Detection: Landscapes, Phase Transitions, and Hardness* (2017), arXiv:1702.00467.
- [31] J. Reichardt and M. Leone, *Physical review letters* **101**, 078701 (2008).
- [32] R. R. Nadakuditi and M. E. J. Newman, *Physical Review Letters* **108**, 188701 (2012).
- [33] X. Zhang, R. R. Nadakuditi, and M. E. J. Newman, *Physical Review E* **89**, 042816 (2014).
- [34] F. Radicchi, *Physical Review E* **88**, 010801 (2013).
- [35] M. B. Hastings, *Physical Review E* **74**, 035102 (2006).
- [36] T. P. Peixoto, *Physical Review X* **4**, 011047 (2014).
- [37] T. P. Peixoto, *Physical Review X* **5**, 011033 (2015).
- [38] T. P. Peixoto, *Physical Review E* **92**, 042807 (2015).
- [39] R. J. Gallagher, J.-G. Young, and B. F. Welles, *Science Advances* **7**, eabc9800 (2021).
- [40] A. Lancichinetti and S. Fortunato, *Physical Review E* **80**, 056117 (2009).
- [41] M. Bazzi, L. G. Jeub, A. Arenas, S. D. Howison, and M. A. Porter, *Physical Review Research* **2**, 023100 (2020).
- [42] E. M. Airoldi, D. M. Blei, S. E. Fienberg, and E. P. Xing, *Advances in neural information processing systems* **21** (2008).
- [43] B. K. Fosdick, D. B. Larremore, J. Nishimura, and J. Ugander, *SIAM Review* **60**, 315 (2018).
- [44] J. Lin, *IEEE Transactions on Information theory* **37**, 145 (1991).
- [45] T. P. Peixoto, figshare 10.6084/m9.figshare.1164194 (2014).
- [46] H. W. Kuhn, *Naval research logistics quarterly* **2**, 83 (1955).
- [47] J. Munkres, *Journal of the society for industrial and applied mathematics* **5**, 32 (1957).
- [48] T. P. Peixoto, *Physical Review X* **12**, 011004 (2022).
- [49] L. Zhang and T. P. Peixoto, *Physical Review Research* **2**, 043271 (2020).
- [50] P. Ramaciotti Morales, in *Complex Networks and Their Applications XI* (Springer International Publishing, Cham, 2023) pp. 176–189.
- [51] S. Boyd, S. P. Boyd, and L. Vandenberghe, *Convex Optimization* (Cambridge university press, 2004).